Distinct mechanisms of iron and zinc metal ions on osteo-immunomodulation of silicocarnotite bioceramics

Fanyan Deng [a,1], Xianzhuo Han [b,1], Yingqi Ji [d], Ying Jin [a], Yiran Shao [e], Jingju Zhang [c,*], Congqin Ning [a,**]

[a] The Education Ministry Key Lab of Resource Chemistry and Shanghai Frontiers Science Center of Biomimetic Catalysis and Shanghai Engineering Research Center of Green Energy Chemical Engineering, Shanghai Normal University, Shanghai, China
[b] Department of Stomatology, Shanghai General Hospital, Shanghai Jiao Tong University School of Medicine, No.100 Haining Road, Shanghai 200080, PR China
[c] Tongji University, Shanghai Engineering Research Center of Tooth Restoration and Regeneration, Department of Orthodontics, School & Hospital of Stomatology, Shanghai, China
[d] State Key Laboratory of High Performance Ceramics and Superfine Microstructure, Institute of Ceramics, Chinese Academy of Sciences, Shanghai, 200050, China
[e] SHNU-YAPENG Joint Lab of Tissue Repair Materials, Shanghai Yapeng Biological Technology Co., Ltd, Shanghai, China

ARTICLE INFO

ABSTRACT

The immunomodulatory of implants have drawn more and more attention these years. However, the immuno-modulatory of different elements on the same biomaterials have been rarely investigated. In this work, two widely used biosafety elements, iron and zinc added silicocarnotite ($Ca_5(PO_4)_2SiO_4$, CPS) were applied to explore the routine of elements on immune response. The immune reactions over time of Fe-CPS and Zn-CPS were explored at genetic level and protein level, and the effects of their immune microenvironment with different time points on osteogenesis were also investigated in depth. The results confirmed that both Fe-CPS and Zn-CPS had favorable ability to secret anti-inflammatory cytokines. The immune microenvironment of Fe-CPS and Zn-CPS also could accelerate osteogenesis and osteogenic differentiation *in vitro* and *in vivo*. In terms of mechanism, RNA-seq analysis and Western-blot experiment revealed that PI3K-Akt signaling pathway and JAK-STAT signaling pathways were activated of Fe-CPS to promote macrophage polarization from M1 to M2, and its immune microenvironment induced osteogenic differentiation through the activation of Hippo signaling pathway. In comparison, Zn-CPS inhibited polarization of M1 macrophage via the up-regulation of Rap1 signaling pathway and complement and coagulation cascade pathway, while its osteogenic differentiation related pathway of immune environment was NF-κB signaling pathway.

1. Introduction

Immune responses were recognized as harmful to host after implantation in the past, hence, bioinert biomaterials were designed to minimize the immune reactions [1]. However, with the importance of immune cells on osteogenesis were found during 1970 s [2], Arron and Choi first proposed the concept of "osteoimmunology" at 2000, which noted T cells can regulate the activities of osteoclasts through secreting RANKL and interferon-γ molecule [3], indicating that appropriate inflammatory reaction can stimulate new bone formation. Afterwards, the effect of inflammatory reaction of bone repair materials on osteogenesis

were investigated widely [4,5]. Among all immune cells, macrophages take an important role in the immune responses induced by biomaterials, which have high plasticity, can easily switching phenotype to another in response to the stimulation, the proinflammatory "M1" and the anti-inflammatory "M2" [6–8]. Moreover, the activation of M1 may suppress the differentiation and collagen synthesis by secreting inflammatory cytokines such as tumor necrosis factor alpha (TNF-α), interleukin 6 (IL-6) and interleukin 1 beta (IL-1β) [9]. In contrast, the anti-inflammatory cytokines including interleukin 4 (IL-4), interleukin 10 (IL-10), interleukin 13 (IL-13) and transforming growth factor-β (TGF-β) produced by M2 macrophages are proven to promote migration

and proliferation of osteoblasts, and inhibit osteoclast formation and bone resorption [10,11]. Hence, various results indicate that stimulating the transformation of macrophages from M1 to M2 phenotype is beneficial for bone formation.

The phenotype of macrophages is well known to be affected by a variety of elements including surface topography and architecture, wettability, chemistry, surface charge or stiffness [12–15]. Likewise, the osteogenic activity of implants can be influenced by these factors [16]. Therefore, it is very necessary to investigate from multiple cells when exploring the osteogenic activity mechanism of bone repair materials. Silicocarnotite(Ca$_5$(PO$_4$)SiO$_4$, CPS) bioceramic is a promising bone repair materials with good biocompatibility, favorable osteogenic activity and biodegradability [17,18]. Our previous works have found that the addition of zinc (Zn) and iron (Fe) elements can significantly improve the mechanical strength and osteogenic ability, the bending strength of 1Zn-CPS and 1Fe-CPS at 1300 °C can up to 80.8 MPa and 88.8 MPa, which are quite equivalent [19,20]. Nevertheless, the mechanism of osteogenic activity only investigated from the perspective of osteoblasts, and only the expression of genes related to osteoblastic differentiation were determined [21,22]. Furthermore, when Zn or Fe was added into CPS, it is an interesting project to investigate the effects of different additives with same weight percentage on osteoimmunology of CPS bioceramic.

Both Zn and Fe, as well known as essential trace elements for many normal physiological functions in humans, play vital role in human body, bone growth and metabolism [23,24]. In addition to the positive effects of Zn and Fe elements on bone regeneration, the effects of Zn and Fe on immune response have also been discussed. Results have shown a promoted expression of pro-inflammatory cytokines including IL-1β, IL-1α and IL-6 with Zn deficiency, indicating Zn deficiency might cause pro-inflammatory response [25–27]. In comparison, the effect of Fe on immune regulation reveals contradictory trends, Fe deficiency have shown influences on the normal functions of immune cells, while Fe supplements have increased death rate of malaria and other health problems [28,29]. Besides, the effect of Fe on osteoimmunology has been rarely studied so far. In this work, the immune reaction over time of Fe-CPS and Zn-CPS were investigated at genetic level and protein level in depth. In addition, the influences and underlying mechanism of immune microenvironment caused by Fe-CPS and Zn-CPS on osteogenesis were also studied *in vitro* and *in vivo*.

2. Materials and methods

2.1. Materials preparation and characterization

To investigate the effect of Fe or Zn addition on bone immunomodulatory ability of CPS bioceramic, 1 wt% Fe$_2$O$_3$ or 1 wt% ZnO were added into CPS and sintered at 1300 °C to prepare Fe-CPS or Zn-CPS bioceramics, and pure CPS ceramics sintered at 1300 °C were used as the control group, while CPS powders were prepared by sol-gel method and calcined at 1350 °C. After sintered, to decrease the effect of surface characteristic on bone immunomodulatory ability, experiments were carried out using extracts of ceramic particle, CPS, Fe-CPS and Zn-CPS bioceramics were ground and sieved to get particles between 20 and 60 mesh. The particles were soaked in DMEM solution at a mass/volume ration of 0.2 g/ml. After soaking 24 h at 37 °C, the extracts were collected and stored at 4 °C. X-ray diffraction (XRD, D/MAX-RBX, Rigaku, Japan) and field-emission scanning electron microscope (FE-SEM, SU8220, HITACHI, Japan) were used to detect the phase composition and morphologies of CPS, Fe-CPS and Zn-CPS particles, respectively. Inductively coupled plasma atomic emission spectroscopy (Vista AXE, Varian, Palo Alto, CA) was used to test the concentration of extracts.

2.2. In vitro experiments

2.2.1. Cell culture

Mouse macrophage cells (RAW 264.7) and rat bone marrow mesenchymal stem cells (rBMSCs) were used to investigate the bone immunomodulatory abilities of samples. RAW 264.7 and rBMSCs were purchased from the Shanghai Institutes for Biological Science, Chinese Academy of Science (Shanghai, China), and cells cultured in DMEM (HyClone) containing 10 % fetal bovine serum (Gibco) and 1 % penicillin/streptomycin (Gibco) at 37 °C with a 5 % CO$_2$ humidified atmosphere. Cells were cultured for 3 days for detection of macrophage polarization.

2.2.2. Immune reaction of RAW 264.7 to Fe-CPS/Zn-CPS at genetic level

2.2.2.1. RNA isolation, RNA-sequencing and bioinformatic data analysis.
To investigate the effect of Fe/Zn addition into CPS on transcription of RNA of RAW 264.7, RNA of RAW 264.7 was extracted using a Qiagen RNeasy® Mini Kit (Qiagen, Hilden, Germany) after culturing with extracts of CPS, Fe-CPS and Zn-CPS for 3 days, respectively, and three parallel samples for each group. After extraction, RNA-sequencing of samples was performed in Genesky Biotechnologies, Inc (Shanghai, China). The heatmap of differentially expressed genes (DEGs) was generated with Heatmap Builder, and gene ontology (GO) and KEGG enrichment analysis were conducted by DAVID software (http://david.abcc.ncifcrf.gov/).

2.2.2.2. Real-time fluorescent quantitative PCR (qRT-PCR) analysis. qRT-PCR analysis was performed to detect the relative gene expression level of RAW 264.7 after culturing with extracts of CPS, Fe-CPS and Zn-CPS for different time, respectively. RAW 264.7 cells were seeded at a density of 5×10^5 cells/cm^2, the cell culture medium was replaced with extracts after 6 h of incubation. After culturing for different time, the relative gene expression levels of RAW 264.7 cells were determined by qRT-PCR including M1 macrophage markers TNF-α, IL-6, CCR7, CD11c, IL-1β, INOS and M2 macrophage markers CD206, IL-4, IL-10, IL-1Ra and Arg1. The sequences of primers are listed in Supplementary Table 1. RAW 264.7 cultured with normal medium were used as control, and relative mRNA levels of the target genes were normalized to glyceraldehyde-3-phosphate dehydrogenase (GAPDH).

2.2.3. Immune reaction of RAW 264.7 to Fe-CPS/Zn-CPS at protein level

2.2.3.1. Enzyme linked immunosorbent assay (ELISA) of secreted cytokines. After culturing with extracts of CPS, Fe-CPS and Zn-CPS for 3 or 5 days, respectively, the culture supernatant of RAW 264.7 was collected. Subsequently, ELISA kits (MultiSciences Biotech, China) were used to measure the concentrations of TNF-α for M1 macrophage marker and IL-10 for M2 macrophage marker in the supernatants.

2.2.3.2. Flow cytometry analysis of polarization markers. Flow cytometry analysis was performed to examine the surface markers of M0 (F4/80), M1 (CD11c) and M2 (CD206) of RAW 264.7 culturing with extracts of CPS, Fe-CPS and Zn-CPS, respectively. After incubation for 1, 2, 3, 4 and 5 days, respectively, cells were collected and incubated with Fluorescein isothiocyanate (FITC)-conjugated anti-F4/80, allophycocyanin (APC)-conjugated CD11c and phycoerythrin (PE)-conjugated CD206 for 30 min at 4 °C. After washing twice, cells were resuspended using DAPI and then transferred into fluorescence activated cell sorting (FACS) tubes, followed analysis was carried out on a flow cytometer (Cytoflex LX, Beckman Coulter). M1-or M2-like macrophages were identified as F4/80-positive/CD11c-positive or F4/80-positive/CD206-positive cells, respectively.
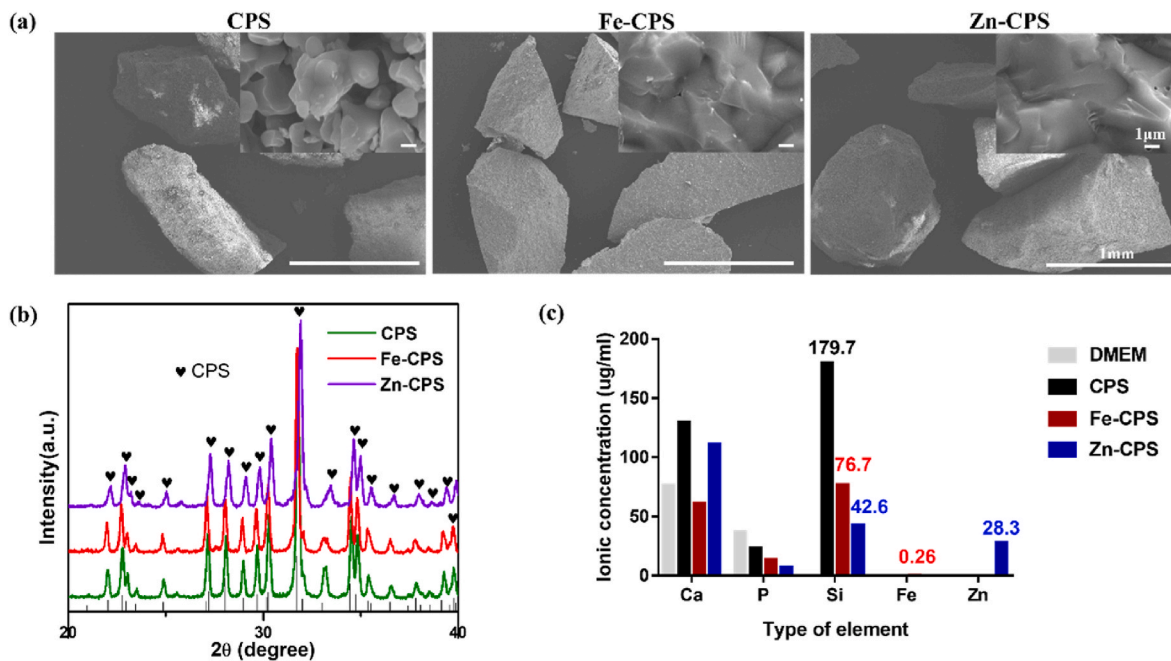
Fig. 1. Characterization of CPS, Fe-CPS and Zn-CPS bioceramics, (a) SEM images, (b) XRD patterns and (c) ions concentration of particle extracts.

2.2.4. Effects of immune microenvironment of Fe-CPS/Zn-CPS on osteogenesis

The effects of immune microenvironment of Fe-CPS or Zn-CPS on osteogenesis was determined by incubating rBMSCs with extracts of CPS, Fe-CPS and Zn-CPS, and macrophage-conditioned culture medium of CPS, Fe-CPS and Zn-CPS, respectively. The immune microenvironment of Fe-CPS or Zn-CPS was prepared in the following steps, after 2 or 4 days of culture with extracts of samples, the supernatant of RAW 264.7 is collected and passed through a 0.22μm filter. Macrophage conditioned medium was prepared by mixing the collected supernatant with complete DMEM medium at a ratio of 1:2, indicated as CPS-CM-2, Fe-CPS-CM-2, Zn-CPS-CM-2, CPS-CM-4, Fe-CPS-CM-4 and Zn-CPS-CM-4, respectively, the extracts of CPS, Fe-CPS and Zn-CPS were used as control. The osteogenic differentiation medium was supplemented with 50 μg/ml ascorbic acid, 10 mM β-glycerophosphate and 100 nM dexamethasone. rBMSCs were seeded in DMEM complete medium for 12 h and then replaced with conditioned medium.

2.2.4.1. Cell proliferation and viability.
The CCK-8 assay was performed to evaluate the proliferation of rBMSCs with samples. Cells were seeded in extracts or immune environment at 1×10^3 per well in 96-well plate. After culturing for 1, 3 and 7 days, the cells were cultured in fresh medium containing 10 % CCK-8 for 2 h at 37 °C. Subsequently, the absorbance was detected at 450 nm with a microplate spectrophotometer (Benchmark Plus, Tacoma, Washington, USA). Cells cultured with normal medium were used as control.

2.2.4.2. ALP activity assay.
After induction with CPS, Fe-CPS, Zn-CPS, CPS-CM-2, Fe-CPS-CM-2, Zn-CPS-CM-2, CPS-CM-4, Fe-CPS-CM-4 and Zn-CPS-CM-4 for 7 days, the activity of ALP of each group was assessed with the Alkaline Phosphatase Assay Kit.

2.2.4.3. ALP and Alizarin red staining.
To investigate the effects of immune environment of Fe-CPS/Zn-CPS on differentiation and calcination of rBMSCs, after inducing for 7 days, the cells were fixed and stained with ALP staining kits (Beyotime, Haimen, Jiangsu, China). After inducing for 14 and 21 days, respectively, the calcified deposits of cells were measured by staining with Alizarin Red (Cyagen Biosciences, Guangzhou, Guangdong, China).

2.2.4.4. RNA isolation and qRT-PCR analysis.
These protocols were the same with the above 2.2.2.2. section. Briefly, after inducing for 3 and 7 days, respectively, the relative gene expression levels of BMP2, ALP, VEGF, OPN, OCN, SP7 and COL1 of CPS, Fe-CPS, Zn-CPS, CPS-CM-4, Fe-CPS-CM-4 and Zn-CPS-CM-4 groups were measured, the sequences of primers were listed in Supplementary. Relative mRNA levels of the target genes were normalized to β-actin, and rBMSCs cultured with neither extracts nor conditioned medium were used as control.

2.2.4.5. Western blot.
Western blot was used to verify the mechanism of the effects of immune environment of Fe-CPS or Zn-CPS on osteogenesis. After incubation, cells were lysed with Radio-Immunoprecipitation Assay (RIPA) buffer (Beyotime, Haimen, Jiangsu, China) and total protein was then quantified by BCA kits (Beyotime, Haimen, Jiangsu, China). Separating proteins, transferring membranes, blocking, incubating and washes was carried out as described previously. The incubated primary antibodies were YAP, P-YAP or α-tubulin (all 1:1000, rabbit anti-mouse; CST) for CPS, CPS-CM-4, Fe-CPS and Fe-CPS-CM-4; phospho–NF–κB p65 (p–NF–κB P-p65, CST#3033) and NF-κB p65 (CST#8242) or α-tubulin (all 1:1000, rabbit anti-mouse) for CPS, CPS-CM-4, Zn-CPS and Zn-CPS-CM-4.

2.3. In vivo experiments

The operation of this animal experiment was approved by the Animal Ethics Committee of Shanghai Normal University. In order to investigate the effect of Fe/Zn addition on the osteoimmune properties of CPS bioceramics at the early stage of implantation, a bone defect model of rat skull was established and implanted with porous CPS, Fe-CPS and Zn-CPS scaffolds. Samples were collected on days 4, 7 and 14 after defect surgery, H&E, Masson staining and immunohistochemical staining for polarization-related INOS, ARG1, and osteogenesis-related OCN were performed.

2.4. Statistical analysis

All data *in vitro* and *in vivo* was from three or more than three experiments. Statistical analysis was performed by GraphPad Prism (GraphPad) using one-way analysis of variance (ANOVA) or Student's t-
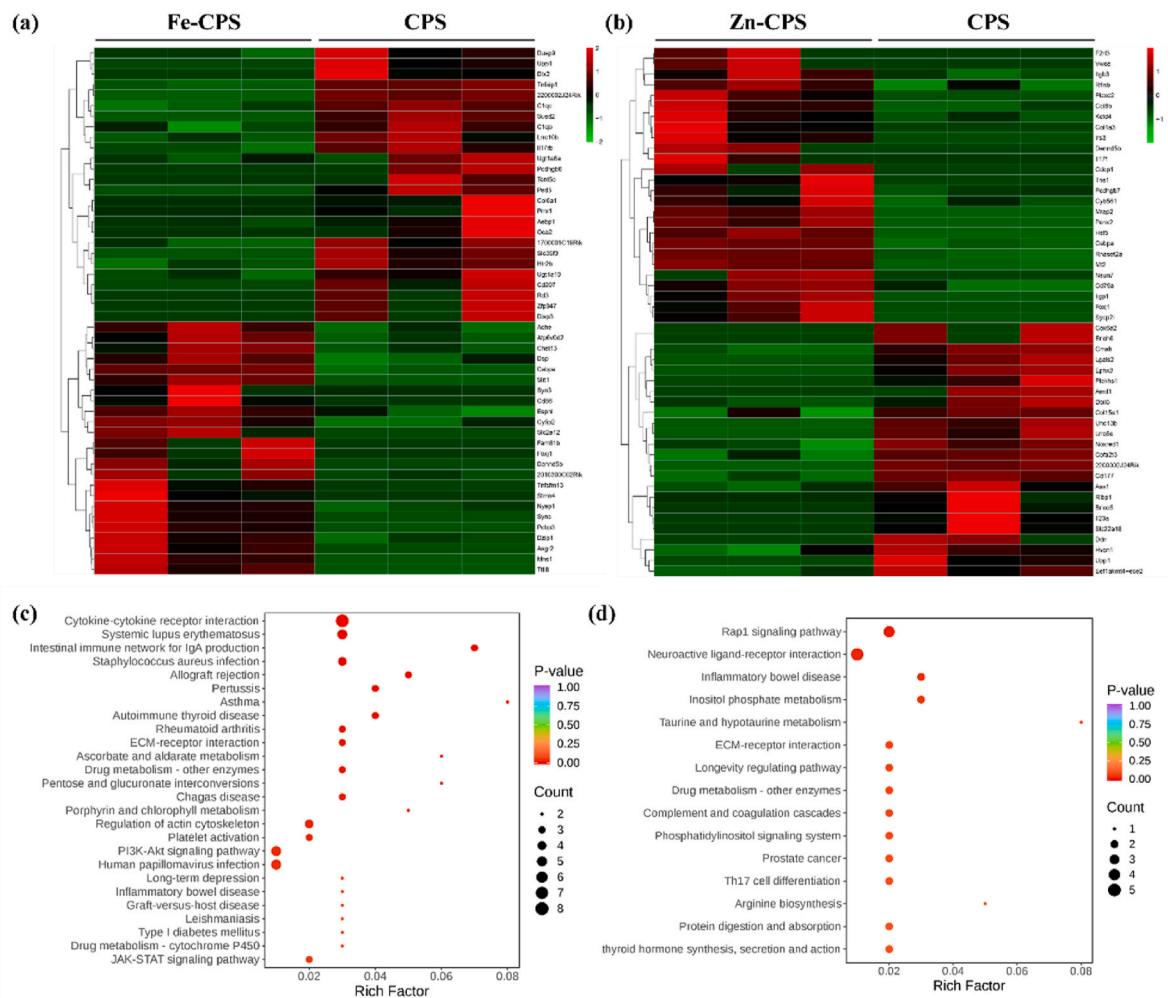
Fig. 2. Analysis of sequencing results of Fe-CPS/Zn-CPS reactions with macrophages with CPS as a control. Heat map of the top 50 DEGs for (a) Fe-CPS, (b) Zn-CPS with CPS, KEGG pathways for (c) Fe-CPS, (d) Zn-CPS with CPS.

test.

3. Results

3.1. Characterization of the bioceramics

Characterization of CPS, Fe-CPS and Zn-CPS bioceramic particles were shown in Fig. 1, the prepared CPS, Fe-CPS and Zn-CPS particles presented the same micron-scale range as shown in Fig. 1(a), and the magnification images showed that all particles had a smooth surface. Besides, a loose and porous structure could be observed of CPS particles, on the other hand, Fe-CPS and Zn-CPS particles had dense surface owing to the addition of Fe_2O_3 and ZnO. XRD patterns of the samples as shown in Fig. 1(b) indicated that both of the main phase of Fe-CPS and Zn-CPS were still CPS, with no other significant peak been detected, which may due to the limitation of XRD detection.

After 24 h of extraction, the ionic concentrations of each group were shown in Fig. 1(c). The ICP results showed that the concentration of Ca, P, Si, Fe and Zn ions in the DMEM significantly changed after immersion. The concentration of Ca and Si ions in the pure CPS extracts were significantly higher compared to DMEM, the concentration of Si ion reached 179.7 μg/ml while the concentration of P ion was slightly reduced. Moreover, the addition of Fe_2O_3 significantly inhibited ions release rate of Ca, P and Si compared to CPS, the concentration of Ca and Si ions in the extract of Fe-CPS particles were less than 1/2 times of them of CPS. On the other hand, the addition of ZnO also inhibited the release

rate of Ca, P and Si compared to CPS, but unlike Fe-CPS, the Ca ion concentration of Zn-CPS extract was only slightly lower than that of CPS, and the concentrations of P and Si ions were much less than them of Fe-CPS.

Besides, when the same mass percentage of Fe_2O_3 or ZnO was added into CPS, the concentration of Fe ion of Fe-CPS was only 0.26 μg/ml while the concentration of Zn ion of Zn-CPS extract was 28.3 μg/ml, which is 109 times of the concentration of Fe ion. The ICP results indicated a significantly difference between Fe-CPS and Zn-CPS.

3.2. Immune response of RAW 264.7 to Fe-CPS/Zn-CPS at genetic level

3.2.1. RNA-sequencing analysis identified differentially expressed genes of RAW 264.7 to Fe-CPS/Zn-CPS

RNA-sequencing was used to identify DEGs of RAW 264.7 treated with Fe-CPS/Zn-CPS, and CPS was used as a control group. RNA-sequencing was performed in three biological replicates with a cut-off criterion of a fold change of more than 2, and a p-value of less than 0.05. When Fe-CPS and CPS groups were compared, 134 DEGs could be detected, including 69 up-regulated and 65 down-regulated DEGs, as shown in the volcano plot (Supplementary Fig. 1). The top 50 DEGs for the Fe-CPS and CPS groups were presented by heat map (Fig. 2(a)). GO analyses were also performed to investigate the function of DEGs, including biological process (BP), cellular components (CC) and molecular function (MF) (Supplementary Fig. 2). The BP analysis indicated that these DEGs were associated with 10 biological processes, including
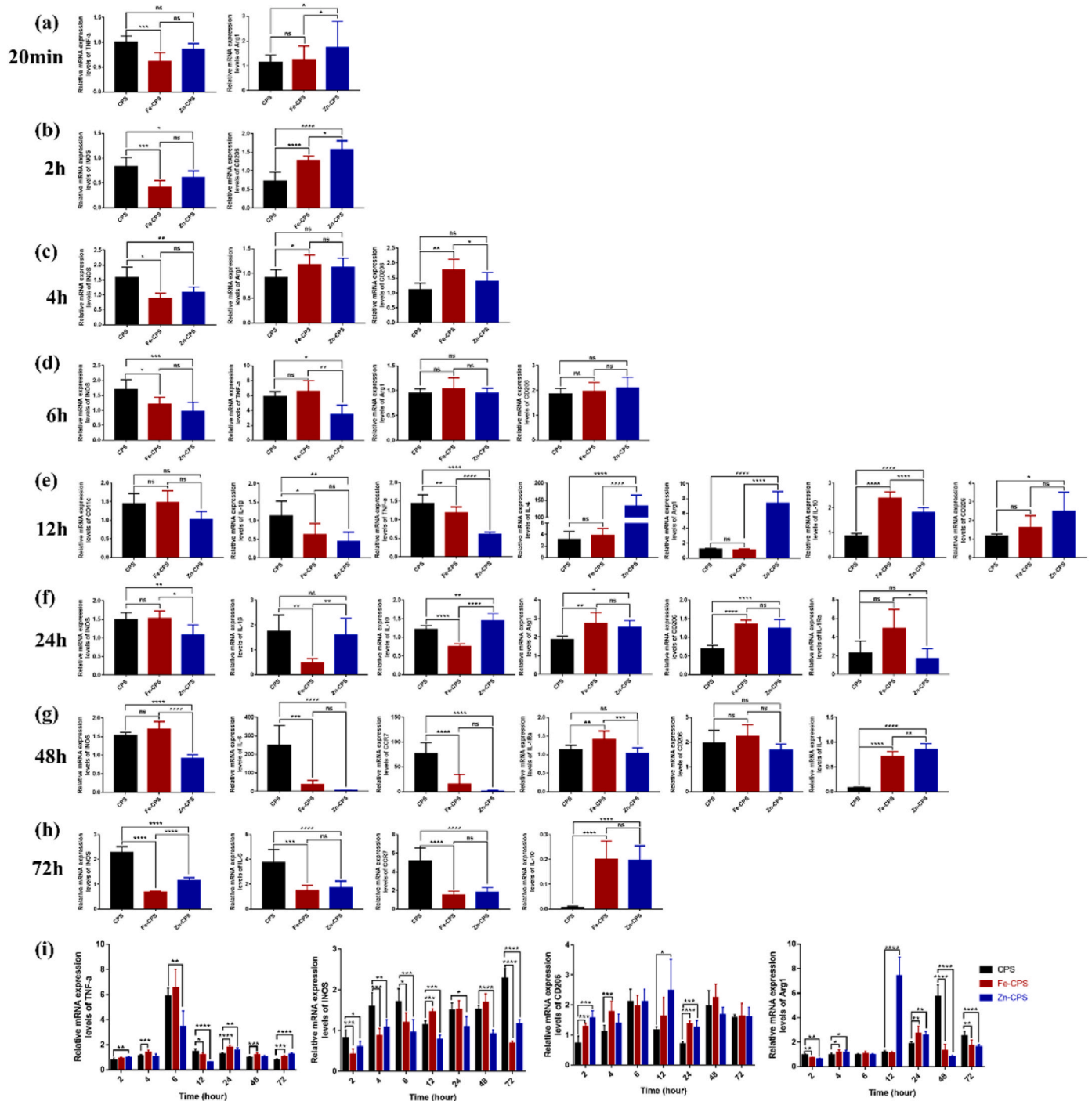
Fig. 3. Relative expression of inflammation-related genes M1, TNF-α, INOS, CD11c, CCR7, IL-1β, IL-6; M2,ARG1, CD206, IL-10, IL-4, IL-1Ra in three groups. RAW 264.7 cultured on tissue culture dishes was taken as control and these values were normalized to the housekeeping gene GAPDH. * indicates statistically significant (P < 0.05) compared to control, while **** indicates P < 0.0001, *** indicates P < 0.001 and ** indicates P < 0.01.

the regulation of the transmembrane receptor protein serine/threonine kinase signaling pathway, negative regulation of monocyte, lymphoid and leukocyte proliferation and positive regulation of endothelial cell proliferation, etc. The molecular function of DEGs including monovalent inorganic cation transmembrane transporter activity, cation symporter activity, proton transmembrane transporter activity, cytokine receptor activity, transforming growth factor beta receptor binding and platelet-derived growth factor binding, etc.

Moreover, the above DEGs were found to be involved in 10 KEGG pathways as shown in Fig. 2(c), including ECM-receptor interaction,

PI3K-Akt signaling pathway, JAK-STAT signaling pathway, rheumatoid arthritis, allograft rejection and cytokine-cytokine receptor interaction, etc.

When Zn-CPS and CPS groups were compared, we eventually identified 105 DEGs, including 56 up-regulated and 49 down-regulated DEGs, as shown in the volcano plot (Supplementary Fig. 3). The top 50 DEGs of Zn-CPS and CPS groups were presented by heat map (Fig. 2 (b)). GO analysis of DEGs was performed including BP, CC and MF (Supplementary Fig. 4). The results of the biological process analysis indicate that these DEGs are closely associated with involvement in
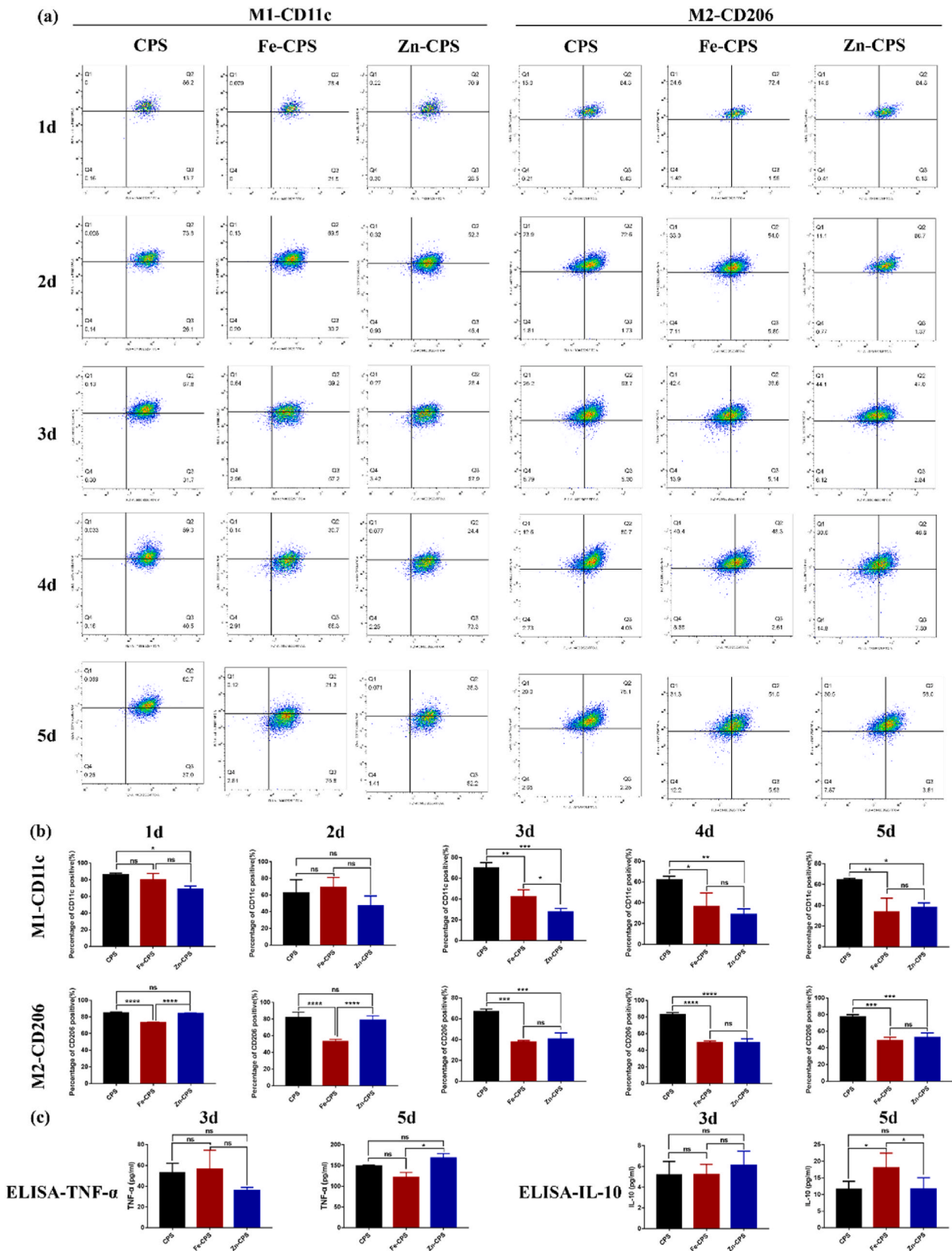
Fig. 4. Percentage of RAW264.7 of (a) (F4/80+, CD11c+) M1 macrophage marker and (F4/80+, CD206+) M2 macrophage marker cells in each group for CPS, Fe-CPS and Zn-CPS at 1, 2, 3, 4 and 5 days, (b) Percentage (%) of CD11c and CD206 positive cells at each time point. * indicates statistically significant (P < 0.05) compared to control, while **** indicates P < 0.0001, *** indicates P < 0.001, and ** indicates P < 0.01. (c) Protein expression levels of macrophage-associated cytokines, including TNF-α, and IL-10 in CPS, Fe-CPS and Zn-CPS-treated supernatants at 3 and 5 days as determined by ELISA, * indicates statistically significant (p < 0.05) compared to control.

fibroblast migration, cellular response to zinc ions, regulation of granulocyte macrophage colony-stimulating factor production, angiogenesis, cell adhesion molecule binding, integrin binding, glycosaminoglycan binding, fibroblast growth factor binding, cytokine-binding G protein-coupled peptide receptor activity, and structural components of the extracellular matrix are closely related. The regulatory process of granulocyte macrophage colony-stimulating factor production may be associated with the migration of BMSC into the region of bone defects. In addition, cell adhesion molecule binding, integrin binding, glycosaminoglycan binding, and CC-acquired membrane rafts, membrane microdomains, membrane zones, receptor complexes, basement membranes, and endocytic vesicles are associated with macrophage adhesion and may further influence the osteogenic role of BMSC.

Moreover, these DEGs were associated with fibroblast growth factor binding, cytokine-binding G protein-coupled peptide receptor activity, and structural components of the extracellular matrix. KEGG analysis was also conducted, which showed that these DEGs were mainly involved in the phosphatidylinositol signaling system as well as inositol phosphate metabolism, Rap1 signaling pathway, complement and coagulation cascades, longevity regulatory pathways, ECM-receptor interactions and neuroactive ligand-receptor interactions, etc (Fig. 2 (d)).

3.2.2. qRT-PCR analysis of genes expression of RAW 264.7 to Fe-CPS/Zn-CPS

The relative gene expression level of RAW 264.7 was determined by qRT-PCR to investigate the expression levels of the M1 macrophage marker TNF-α, IL-6, CCR7, CD11c, IL-1β and INOS; M2 macrophage marker, CD206, IL-4, IL-10, IL-1Ra and Arg1. qRT-PCR was performed at different time points (20min, 2 h, 4 h, 6 h, 12 h, 24 h, 48 h, 72 h) on the genes related to macrophage polarization induced by Fe-CPS and Zn-CPS, and CPS was used as control.

After cultured for 20 min, both Fe-CPS and Zn-CPS started to show a trend towards an inhibiting effect of pro-inflammation and a promotion of anti-inflammation as shown in Fig. 3(a). Compared to CPS, both Fe-CPS and Zn-CPS groups showed down-regulation of the relative expression of TNF-α, with a significant down-regulation in Fe-CPS group ($p < 0.05$), while the Zn-CPS group only showed a modest down-regulation. Moreover, Fe-CPS and Zn-CPS also promoted the relative expression of ARG1 at 20 min, with a significant difference in the Zn-CPS group ($P < 0.05$), while the Fe-CPS group showed a slight up-regulation in the trend.

At 2 h, Fe-CPS and Zn-CPS also showed a diminution of pro-inflammation and a stimulation of anti-inflammation as shown in Fig. 3(b). Both Fe-CPS and Zn-CPS groups showed down-regulation of the relative expression of INOS, with a significant down-regulation in Fe-CPS group ($p < 0.05$). For M2, the relative expression of CD206 in Fe-CPS and Zn-CPS groups was elevated and showed significant differences ($p < 0.05$).

At 4 h, the relative expression of INOS, ARG1 and CD206 of Fe-CPS and Zn-CPS had the same trend with the culture time were 20min and 2 h as shown in Fig. 3(c). The relative expression of both TNF-α and INOS was down-regulated in Zn-CPS group at 6 h with a significant difference ($P < 0.05$), and the relative expression of INOS was down-regulated in Fe-CPS group with a significant difference ($P < 0.05$), while the promotion extent of Fe-CPS and Zn-CPS groups on the relative expression of ARG1 and CD206 started to decrease as shown in Fig. 3(d).

As the co-culture time increased to 12 h as shown in Fig. 3(e), Fe-CPS and Zn-CPS presented inhibitory or promoting effects on more genes. For M1 pro-inflammatory genes, besides TNF-α, ARG1 and CD206, there was a certain down-regulation of the relative expression of IL-1β and CD11c in both Fe-CPS and Zn-CPS groups. For M2 anti-inflammatory genes, the relative expression of IL-10 and IL-4 in Fe-CPS and Zn-CPS groups were all elevated and significantly different ($P < 0.0001$), especially, the relative expression of IL-4 in Zn-CPS groups were up-regulated up to about 40-fold, while Fe-CPS group only showed slight

up-regulation in trend, with no significant difference.

The results after 24 h co-culture as shown in Fig. 3(f) also presented excellent "anti-pro-inflammatory and pro-*anti*-inflammatory" effects. The relative expression of IL-1β and INOS was down-regulated in Fe-CPS and Zn-CPS group, with significant differences ($P < 0.05$). The relative expressions of IL-10, IL-4, CD206 and ARG1 were all elevated and significantly different in Zn-CPS group ($P < 0.05$), while the relative expressions of IL-4, CD206 and IL-1Ra were all elevated and significantly different in Fe-CPS group ($P < 0.05$).

When the incubation time increased to 48 h (Fig. 2(g)), both Fe-CPS and Zn-CPS groups had a significant down-regulation of the relative expression of IL-6 and CCR7 and a remarkable increase in the expression of IL-4, both of which were significantly different ($p < 0.0001$) as shown in Fig. 3(g). At 72 h, Fe-CPS and Zn-CPS presented an inhibition on pro-inflammation, the relative expression of IL-6, INOS and CCR7 were down-regulated in Fe-CPS and Zn-CPS groups with a significant difference ($p < 0.05$), and only a promotion of the expression of IL-10 for M2 as shown in Fig. 3(h).

Overall, Zn-CPS had a significant M2 polarizing effect at the early phase, the expression of ARG1 and CD206 at 20min and 2 h in Zn-CPS were much higher than those in the other two groups, CPS and Fe-CPS. At 12 h, Zn-CPS group produced a 30-40-fold elevation in the relative expression of IL-4 to CPS group, while the expression of ARG1 was as much as six times higher than that of CPS and Fe-CPS groups. The expression of IL-10 at 24 h was also significantly higher in Zn-CPS than in the other two groups($p < 0.05$). The expression of IL-4 at 48 h was also significantly greater in Zn-CPS than in the other two groups, CPS and Fe-CPS ($p < 0.05$).

Compared to Zn-CPS, Fe-CPS induced a slightly weaker effect on the polarization of macrophages towards M2. Specifically, the expression of CD206 at 4 h was significantly higher than in the other two groups, CPS and Zn-CPS ($p < 0.05$), the expression of IL-10 at 12 h and IL-1Ra at 24 h and 48 h was also significantly higher in Fe-CPS group than in the other two groups($p < 0.05$).

Moreover, Fe-CPS and Zn-CPS showed similar trends in the regulation of M1. The inhibition of TNF-α and INOS of Fe-CPS was superior to that of Zn-CPS at early stages of incubation (20 min, 2 h and 4 h). As the incubation time continued to increase, Zn-CPS began to show a better inhibitory effect on M1.

The changes of the relative expressions of M1 markers (TNF-α and INOS), and M2 markers (CD206 and ARG1) with increasing cultivation time for both Fe-CPS and Zn-CPS groups were investigated and the results were shown in Fig. 3(i). It could be found that at the early stage of incubation (6 h and 12 h), Fe-CPS had no significant inhibitory effect on TNF-α, whereas, Zn-CPS significantly inhibited the expression of TNF-α. Moreover, both Fe-CPS and Zn-CPS had a clearly down-regulation effect on INOS, and the down-regulation was more obvious at the early stage (2 h and 4 h) in Fe-CPS group, while Zn-CPS had a more significant down-regulation effect in the middle-late stages of incubation.

In addition, both Fe-CPS and Zn-CPS exhibited a beneficial effect on the expression of M2 marker of CD206. For ARG1, Fe-CPS and Zn-CPS showed a moderate promotion effect at the middle of the incubation period (12 h and 24 h), and the expression of ARG1 of RAW 264.7 culturing with Zn-CPS reached its peak at 12 h. Notably, pure CPS group also exhibited a peak in the expression of ARG1 at 48 h, which may indicate the excellent anti-inflammatory effect of pure CPS.

3.2.3. Flow cytometry analysis of polarization markers of RAW 264.7 to Fe-CPS/Zn-CPS

To investigate the influence of Fe-CPS or Zn-CPS on the classical M1 and M2 markers of macrophages, flow cytometry was used to analyze the expression of the surface markers (CD11c and CD206), time points of 1, 2, 3, 4 and 5 days were chosen. The F4/80-FITC+, CD11c-APC + cell subpopulation was recorded as M1 polarization and the F4/80-FITC+, CD206-PE + cell subpopulation was recorded as M2 polarization.

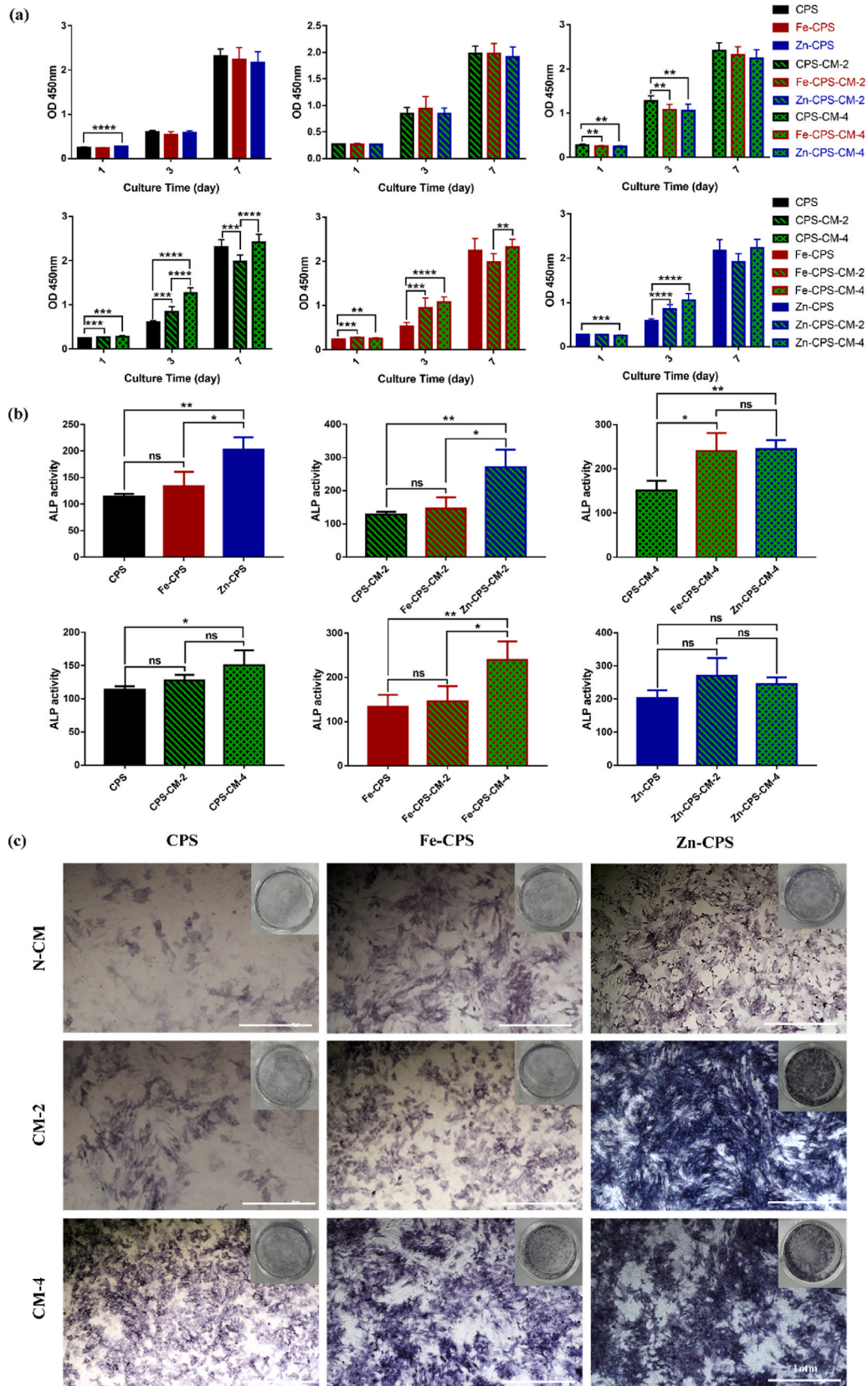The results as shown in Fig. 4(a) indicated that both Fe-CPS and Zn-

Fig. 5. Results of the effects of CPS, CPS-CM-2, CPS-CM-4, Fe-CPS, Fe-CPS-CM-2, Fe-CPS-CM-4, Zn-CPS, Zn-CPS-CM-2 and Zn-CPS-CM-4 on rBMSCs, (a) proliferation, (b) quantification of ALP activity and (c) ALP staining. * indicates statistical significance (P < 0.05), **** indicates P < 0.0001, *** indicates P < 0.001 and ** indicates P < 0.01.

CPS groups reduced the proportion of CD11c positive cells. For Zn-CPS, the proportion of CD11c positive cells was significantly lower than that in CPS group at 1 d, with a significant difference (P < 0.05), and the difference between Zn-CPS and CPS of CD11c positive cells was the largest at 3 d. Besides, the proportion of CD11c positive cells in Zn-CPS was lower than that in CPS at 1-4 d, indicating Zn-CPS may had a better "anti-pro-inflammatory" ability than Fe-CPS. For Fe-CPS, the proportion of CD11c-positive cells was obviously lower than that in CPS until the third day, with a significant difference (P < 0.05). At 5 d, the proportion of CD11c positive cells in Fe-CPS group was not only lower than that in CPS group, but also began to show a trend lower than that in Zn-CPS group, indicating that the immune response of Fe-CPS and Zn-CPS may presented differently owing to the addition of Fe and Zn. Surprisingly, Fe-CPS and Zn-CPS groups did not reach the proportion of CD206-positive M2 macrophage in CPS group at the selected time points, but the proportion of CD206-positive cells was significantly higher in Zn-CPS group compared to Fe-CPS group at 1st and 2nd day, with a significant difference (p < 0.05). With the increase of culture time, the proportion of CD206-positive cells in Fe-CPS and Zn-CPS groups was basically same at 3 d, 4 d and 5 d, and was lower than that in CPS group.

Overall, Fe-CPS, Zn-CPS and CPS all reduced the percentage of positive cells for the M1 marker of CD11c to some extent, with Zn-CPS group showed better effects at early stage, which was consistent with the qRT-PCR trend. With the increase of incubation time, both Fe-CPS and Zn-CPS could decrease the proportion of CD11c positive cells. Whereas for the percentage of positive cells for CD206, Zn-CPS significantly outperformed Fe-CPS group at 1 d and 2 d (p < 0.05), but Fe-CPS and Zn-CPS could not reach the proportion of CD206-positive M2 macrophage in CPS group at the selected time points, and at 3 d-5d, no significant difference was found between the percentage of CD206 positive cells for Fe-CPS and Zn-CPS.

3.2.4. ELISA analysis of secreted cytokines of RAW 264.7 to Fe-CPS/Zn-CPS

To further confirm the phenotype switch of RAW264.7, ELISA was employed to determine the concentrations of TNF-α and IL-10. The results were presented in Fig. 4(c), it could be seen that Zn-CPS achieved effects of "anti-pro-inflammatory and pro-*anti*-inflammatory" earlier than Fe-CPS. At 3 d, the content of pro-inflammatory factor of TNF-α secreted by Zn-CPS was significantly lower than that of CPS and Fe-CPS, and the content of anti-inflammatory factor of IL-10 was also higher than that of CPS and Fe-CPS. In contrast, Fe-CPS achieved "anti-pro-inflammatory and pro-*anti*-inflammatory" effect at the ELISA level until the 5th day. At 5 d, the content of the pro-inflammatory factor of TNF-α secreted by Fe-CPS was significantly lower than that of CPS and Zn-CPS, and the content of anti-inflammatory factor of IL-10 was also higher than that of CPS and Zn-CPS, which further verified distinct immune response of Fe-CPS and Zn-CPS.

Due to the fast release of zinc ions, the concentration in the extract reached 28.3 μg/ml, while the slower release of iron ions, the concentration in the extract was only 0.26μg/ml. The same trend was observed for TNF-α, which was seen to be lower in the Zn-CPS group than in the CPS and Fe-CPS groups at 3 d. In turn, at 5 d, the secretion of pro-inflammatory factors was lower in Fe-CPS group than in Zn-CPS and CPS groups.

It is therefore believed that the level of metal ion concentration contributes to the temporal phase of the anti-inflammatory effect of the material, higher concentrations of ions produce faster effects, while lower concentrations take longer to act or can produce similar anti-inflammatory effects.

3.3. Effects of immune microenvironment of Fe-CPS/Zn-CPS on osteogenesis of rBMSCs

The results of the interaction between Fe-CPS/Zn-CPS bioceramics and macrophages indicated that Fe-CPS and Zn-CPS triggered different immune responses at different time points, the supernatant was therefore collected on the 2nd and 4th day to prepare the immune microenvironment. Therefore, there are nine groups of CPS, CPS-CM-2, CPS-CM-4, Fe-CPS, Fe-CPS-CM-2, Fe-CPS-CM-4, Zn-CPS, Zn-CPS-CM-2 and Zn-CPS-CM-4. The rBMSCs were cultured with nine groups, respectively, and a comparison of the results of different materials under the same culture conditions, as well as a comparison of the effects of different immune microenvironments on cell proliferation for the same material, were shown in Fig. 5(a). The results showed that the extracts of CPS, Fe-CPS and Zn-CPS groups all showed good cytocompatibility, and cell viability increased with increasing culture time, with no significant difference between three groups. The same trend was observed for the groups CPS-CM-2, Fe-CPS-CM-2 and Zn-CPS-CM-2 and for the groups CPS-CM-4, Fe-CPS-CM-4 and Zn-CPS-CM-4, which suggested that the addition of Fe and Zn elements and the immune microenvironment generated by Fe-CPS and Zn-CPS had no negative side effects on the good cytocompatibility of CPS bioceramic, all of which were beneficial to the proliferation of rBMSCs.

Comparing CPS, CPS-CM-2 and CPS-CM-4, Fe-CPS, Fe-CPS-CM-2 and Fe-CPS-CM-4, and Zn-CPS, Zn-CPS-CM-2 and Zn-CPS-CM-4, the three groups still showed the same trend, at the early stage of culture (1–3 d), the immune microenvironment of CPS, Fe-CPS and Zn-CPS bioceramics all contributed to the proliferation of rBMSCs, and the immune microenvironment of 4 days was the most effective in promoting proliferation with significant difference (P < 0.001). Whereas the 2-day immune microenvironment of samples suppressed further cell growth to some extent at 7 d as the incubation time continued to increase, and no significant difference was observed between the 4-day immune microenvironment and the extract alone.

To investigate the effects of immune microenvironment of Fe-CPS/Zn-CPS on the early osteogenic differentiation ability of rBMSCs, the ALP activity of each group was analyzed quantitatively after 7 d of culture, and the results were shown in Fig. 5(b). When compared between three materials, CPS, Fe-CPS and Zn-CPS, the ALP activity was Zn-CPS > Fe-CPS > CPS, indicating that the addition of Zn elements accelerated the differentiation of rBMSCs towards osteogenesis. The ALP activity between CPS-CM-2, Fe-CPS-CM-2 and Zn-CPS-CM-2 groups was Zn-CPS-CM-2 > Fe-CPS-CM-2 > CPS-CM-2, in agreement with the trend of the materials-only group. As the duration of the immune reaction increased, the ALP activity of Fe-CPS-CM-4 group was comparable to that of Zn-CPS-CM-4 group and all were significantly better than that of CPS-CM-4 when comparisons were made between CPS-CM-4, Fe-CPS-CM-4 and Zn-CPS-CM-4 groups.

Analyses of the impact of different immune reaction durations on ALP activity, for pure CPS, the immune microenvironment of CPS bioceramic was favorable to osteogenic differentiation and that the CPS-CM-4 group had the optimum ALP activity. ALP activity of the immune microenvironment of Fe-CPS also exhibited a trend of Fe-CPS-CM-4 > Fe-CPS-CM-2 > Fe-CPS, and the ALP activity of Fe-CPS-CM-4 group was significantly better than that in the other two groups with significant difference (P < 0.05), which suggested that the increase of immune reaction duration benefited the osteogenic differentiation in Fe-CPS group. Regarding Zn-CPS, the Zn-CPS-CM-2 group showed the best ALP activity, and the increase of immune response duration instead led to a moderate decrease in ALP activity, thereby presuming that the long-term immune microenvironment was not conducive to osteogenic differentiation of Zn-CPS bioceramic.

The ALP staining results followed the same trend as the quantitative ALP analysis as shown in Fig. 5(c), the addition of Fe or Zn could further enhance the osteogenic differentiation ability of CPS bioceramic, while Zn-CPS presented the greatest ability to contribute to osteogenic differentiation. Furthermore, the immune microenvironment of three materials, CPS, Fe-CPS and Zn-CPS, was favorable to osteogenic differentiation, with an increase in immune reaction period being favorable to an increase in ALP activity for CPS and Fe-CPS bioceramics, resulting in the darkest color in CPS-CM-4 and Fe-CPS-CM-4 groups,
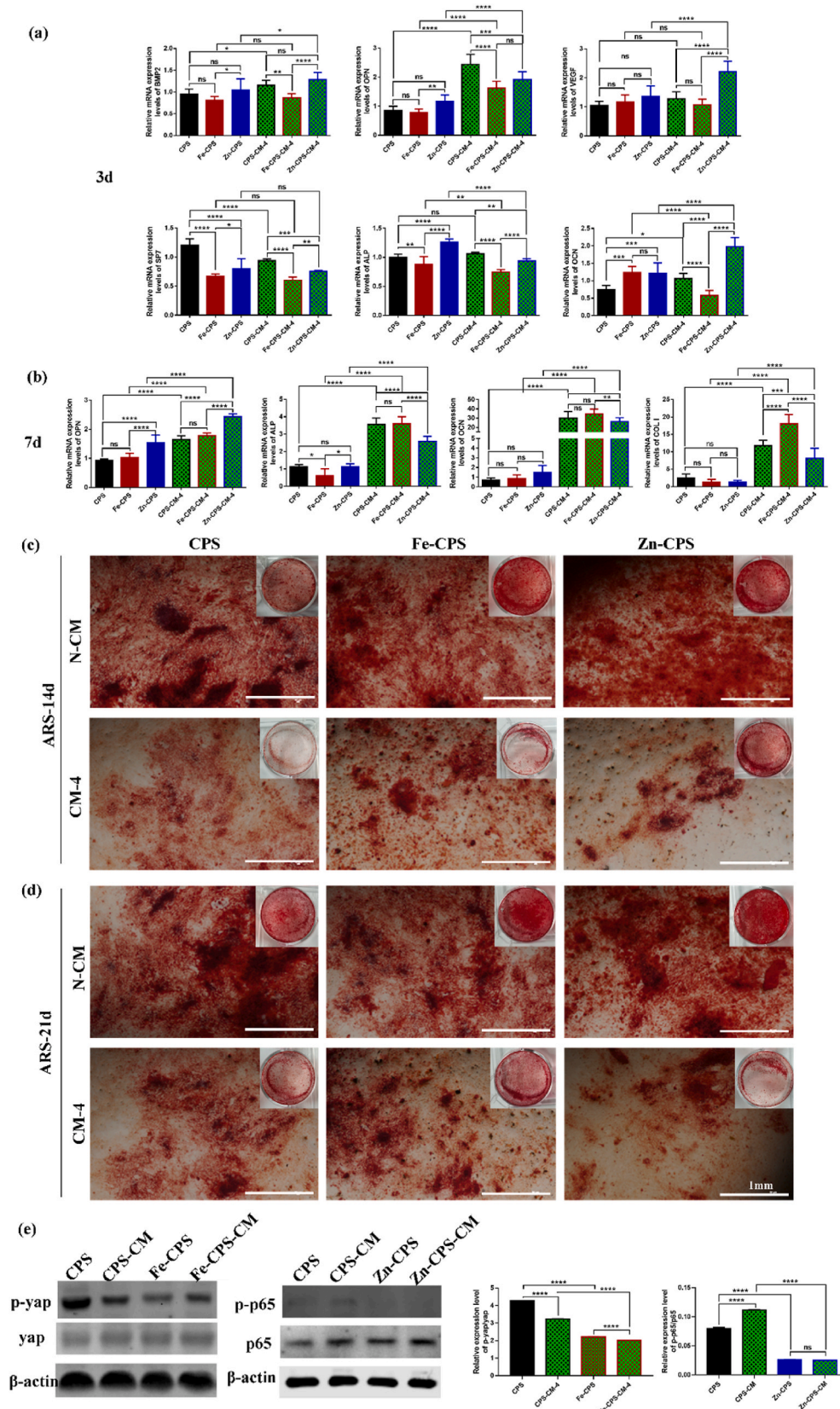
Fig. 6. Results of the effects of CPS, CPS-CM-4, Fe-CPS, Fe-CPS-CM-4, Zn-CPS and Zn-CPS-CM-4 on the osteogenesis of rBMSCs, (a) 3-day, (b) 7-day osteogenic differentiation-related genes expression, (b) 14-day, (d) 21-day ARS staining and (e) Western blot banding and grey-scale calculations. * indicates statistical significance (P < 0.05), **** indicates P < 0.0001, *** indicates P < 0.001 and ** indicates P < 0.01.
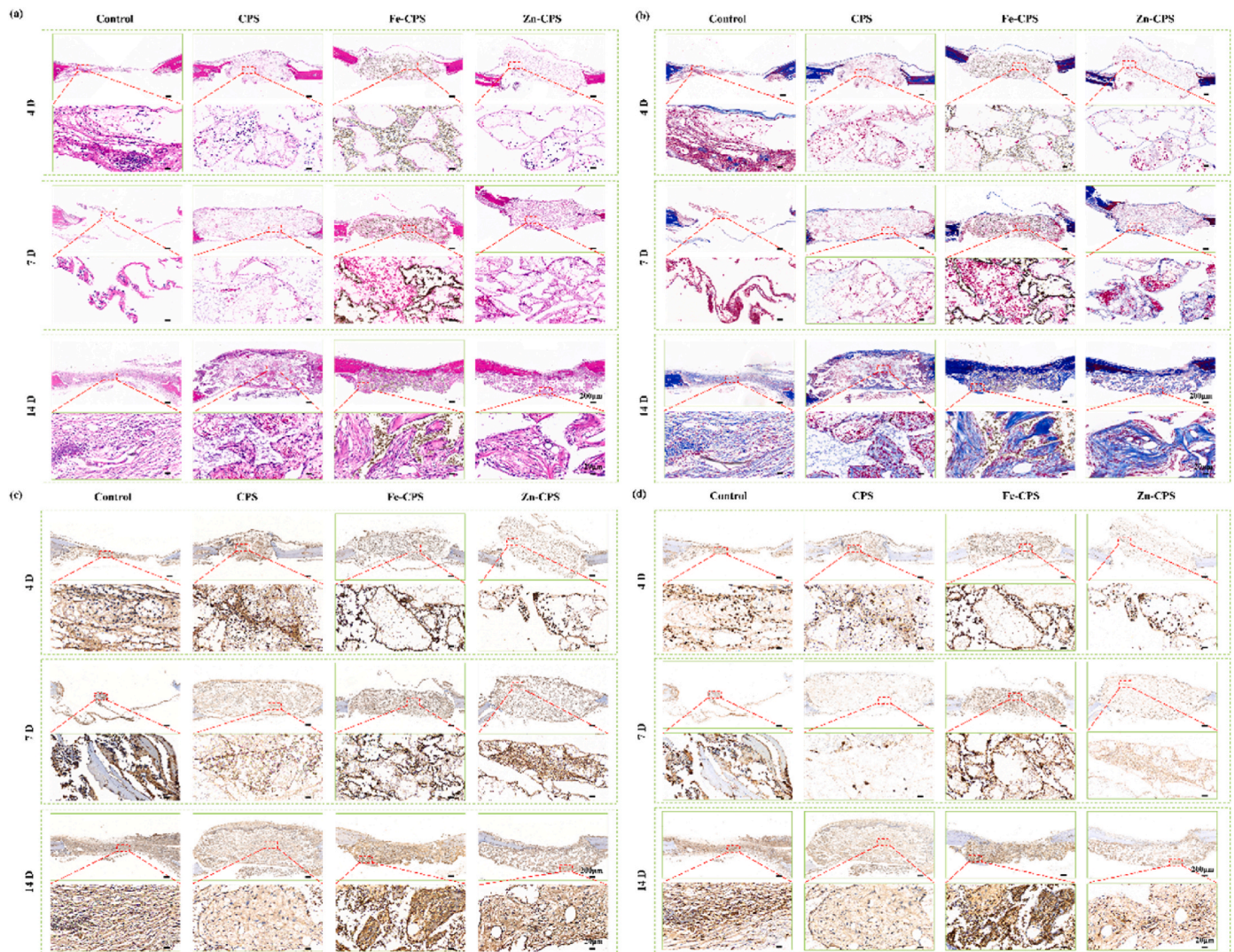
Fig. 7. *In vivo* results of CPS, Fe-CPS and Zn-CPS scaffolds implanted for 4, 7 and 14 days, (a) HE staining, (b) Masson staining, immunohistochemical staining of (c) NOS2 and (d) Arg1.

while the darkest ALP staining in the Zn-CPS-CM-2 group for Zn-CPS material group. When the nine groups were compared, the Zn-CPS-CM-2 group showed the darkest ALP staining, followed by the Zn-CPS-CM-4 and Fe-CPS-CM-4 groups, further demonstrating that Zn-CPS and Fe-CPS and their immune microenvironment are beneficial for osteogenic differentiation.

Given that the immune microenvironment with an immune response duration of 4 days had the best promotion on the osteogenic differentiation of rBMSCs, the 4-day immune microenvironment was chosen for subsequent experiments to investigate the osteogenic differentiation promotion mechanism in depth.

Two time points (3 d and 7 d) were selected to detect the expression of osteogenic genes, as shown in Fig. 6(a) and (b). At 3 d, for the material groups, Zn-CPS group had the optimum ability to promote the expression of BMP2, OPN, VEGF and ALP, while Fe-CPS group could significantly promote the expression of OCN, and CPS could obviously promote the expression of SP7, indicating that all three materials were beneficial to osteogenic differentiation of rBMSCs. With respect to the immune microenvironment of the materials, both CPS-CM and Zn-CPS-CM favored the expression of genes related to osteogenic differentiation, with the highest expression of BMP2, VEGF and OCN in Zn-CPS-CM-4 group and the best promotion effects on OPN, SP7 and ALP expression by CPS-CM-4 as shown in Fig. 6(a). At 7 d, the promotion effect of

immune microenvironment of CPS, Fe-CPS and Zn-CPS on the expression of genes related to osteogenic differentiation of rBMSCs all were better than that of the pure material group, especially the expression of ALP, OCN and COL1. In addition, the expression of OPN was found to be the highest in Zn-CPS-CM-4 group, while the bone differentiation ability of Fe-CPS-CM-4 group was significantly enhanced after 7 days of culture, with the greatest promotion effect on the expression of ALP, OCN and COL1.

Two time points, 14 d (Fig. 6(c)) and 21 d (Fig. 6(d)) were chosen to compare the mineralization of rBMSCs treated with the immune microenvironment or the materials alone, respectively. As could be seen, CPS, Fe-CPS and Zn-CPS groups all facilitated the mineralization of rBMSCs, with pronounced mineralization in all material groups at 14 days, and the overall mineralization at 21 d was greater than those at 14 d. In general, the mineralization capacity of material groups was superior to those of the immune microenvironment groups, and the Zn-CPS-CM-4 group had the weakest mineralization capacity, suggesting that the immune microenvironment accelerates osteogenesis and osteogenic differentiation during the early stages, while it is not beneficial for long-term osteogenic differentiation.

To further determine the intrinsic mechanism of Fe-CPS-CM and Zn-CPS-CM promoting osteogenic differentiation of rBMSCs, the Hippo signaling pathway activation of Fe-CPS-CM and the nuclear factor-κB

(NF-κB) signaling pathway activation of Zn-CPS-CM were detected, yap and its phosphorylation, p65 and its phosphorylation were analyzed by Western blot, and the grey-scale values of the Western blot bands were obtained by ImageJ. The percentage of phosphorylated and non-phosphorylated protein grey values were calculated as in Fig. 6(e). From the percentage of phosphorylated proteins in the grey-scale values, the phosphorylation of yap was significantly lower in Fe-CPS, Fe-CPS-CM compared to CPS and CPS-CM, indicating that the Hippo signaling pathway was being activated in Fe-CPS and Fe-CPS-CM groups, and the phosphorylation of p65 was significantly reduced in the rBMSCs of Zn-CPS and Zn-CPS-CM, indicating that the NF-κB signaling pathway was being activated in the Zn-CPS and Zn-CPS-CM groups. suggesting that the NF-κB signaling pathway was suppressed in Zn-CPS and Zn-CPS-CM groups.

3.4. Osteo-immunomodulation of Fe-CPS and Zn-CPS bioceramics in vivo

The four groups, blank control, CPS, Fe-CPS and Zn-CPS scaffolds were implanted into a skull defect of SD rat model for 4, 7 and 14 days. HE staining, Masson staining and immunohistochemical staining of OCN were used to evaluate the osteogenesis of scaffolds in vivo, and the results were shown in Fig. 7(a) and (b) and Supplementary Fig. 5. At 4 days, the trends of new bone formation were CPS > Zn-CPS > Fe-CPS > Control, while the number of positive cells in immunohistochemical staining of OCN were CPS > Control > Zn-CPS > Fe-CPS. After implantation for 7 days, Zn-CPS and Fe-CPS started to exhibit advantages on osteogenesis, while the trends of new bone formation were Zn-CPS > Fe-CPS > CPS > Control, and the number of positive cells in immunohistochemical staining of OCN were Fe-CPS > Zn-CPS > CPS > Control. At 14 days, the new bone formation of CPS, Fe-CPS and Zn-CPS groups were much better than that of Control group, while Fe-CPS was the highest and followed by Zn-CPS group, and the number of positive cells in immunohistochemical staining of OCN were Fe-CPS > Zn-CPS > CPS > Control.

To detect the immune microenvironment among defect area after implantation, the immunohistochemical staining of M1 macrophage marker, NOS2, and M2 macrophage marker, Arg1 were performed and shown in Fig. 7(d) and (e). At 4 days, the number of positive cells in immunohistochemical staining of NOS2 and Arg1 both presented a trend of CPS > Control > Zn-CPS > Fe-CPS, indicating the implantation of Zn-CPS and Fe-CPS clearly reduced inflammatory reaction. After implanted for 7 days, barely no inflammatory reaction could be observed among all groups, the number of positive cells in immunohistochemical staining of NOS2 and Arg1 obviously decreased, only the number of positive cells in immunohistochemical staining of Arg1 of Fe-CPS was higher than other groups. At 14 days, the number of positive cells in immunohistochemical staining of NOS2 and Arg1 both presented a trend of Fe-CPS > Zn-CPS > Control > CPS, implying an intimate relationship between immune microenvironment and osteogenesis.

4. Discussion

Osteoimmunology has attracted much attention since the close relationship be discovered between immune response and osteogenic capacity, and people gradually realized that regulating the composition of biomaterials can promote bone formation via building a beneficial immune microenvironment. To investigate the osteo-immunomodulation mechanisms of Fe and Zn elements, in present study, we selected novel CPS as research object and investigated osteoimmunology of Fe-CPS and Zn-CPS bioceramics. In addition, the immune response and osteogenic immune microenvironment of Fe-CPS and Zn-CPS were systematically studied, and the underlying mechanism were also explored in vitro and in vivo.

We firstly prepared Fe-CPS (1 wt% Fe$_2$O$_3$ added CPS) and Zn-CPS (1 wt% ZnO added CPS) bioceramics, to decreased the influences of porosity and surface characteristics, bioceramics were ground to

particles with same sizes and then made extracts of Fe-CPS and Zn-CPS as shown in Fig. 1. The concentration of Fe and Zn ions were 0.26 and 28.3 μg/ml respectively, which presented substantially different. The phase composition of Fe-CPS and Zn-CPS have been explored in our previous works, while Fe-CPS are composed of CPS, Fe$_2$O$_3$ and α′-CaSiO$_3$, and Zn-CPS consists of CPS and Ca$_2$ZnSi$_2$O$_7$ [20,30]. The release trends of Fe and Zn after adding into bioceramics are consistent with our results in some studies. The concentration of Zn in Ca$_2$Zn-Si$_2$O$_7$-PLA after soaking in PBS for 24 h is 13.4 μg/ml [31], and the concentration of Zn of 0.5 % aspartic acid and 2 % Ca$_2$ZnSi$_2$O$_7$ ceramic soaking in deionized water for 10 min is 10.2 μg/ml [32], indicating the release of Zn in bioceramics is relatively fast. In contrast, the concentration of Fe in 40F10BGC (40 % F10BG (Bioglasses containing 10 wt% iron)/Chitosan) after soaking in PBS for 14 days is only 2.5 μg/ml [33], suggesting the release of Fe in Ca–P–Si biomaterials is comparatively slow.

Gene is known to responsible for the regulation of protein synthesis, thus, we began the immune response of RAW 264.7 to Fe-CPS/Zn-CPS at genetic level, DEGs of RAW 264.7 treated with Fe-CPS/Zn-CPS were compared with CPS, respectively. The results as shown in Fig. 2 and Supplementary Fig. 1- Fig. 4, the expression of 134 genes and 105 genes were changed owing to the addition of Fe and Zn, respectively. Among GO enrichment and KEGG pathway analyses, both the addition of Fe and Zn changed immune response behavior and subsequent cell behaviors. For Fe-CPS compared with CPS, negative regulation of leukocyte, lymphocyte and mononuclear cell can significantly reduce the immune inflammatory reaction. Cytokine activity and cytokine receptor activity, as well as cytokine-cytokine receptor interaction pathway, are associated with macrophage adhesion and may further influence the osteogenic effect of BMSC [34]. In addition, ECM-receptor interaction pathway can also regulate cellular behaviors including adhesion, proliferation and differentiation [35]. Specially, PI3K-Akt signaling pathway and JAK-STAT signaling pathway, key pathways in regulating polarization of macrophages, were activated in the DEGs of Fe-CPS with CPS. Both PI3K-Akt signaling pathway and JAK-STAT signaling pathway play important roles in mediating cell growth, proliferation, differentiation and apoptosis [36–38], evidences have proven that the down-regulation of PI3K-Akt signaling pathway can inhibit inflammation by promoting macrophage polarization from M1 to M2 [39–42], and IL-10 can up-regulate JAK-STAT signaling pathway to promote M2 polarization through binding surface receptors to activate JAK/STAT3 pathway [43,44]. In this work, the deceased expression of Itga8, Fgfr3, Col6a1, Col1a2 and Il7 as shown in Supplementary Fig. 6 could activate PI3K-Akt signaling pathway, and the increased expression of IL-10 as shown in Supplementary Fig. 7 could activate JAK-STAT signaling pathway. Above all, Fe-CPS can modulate macrophage polarization to M2 through activating PI3K-Akt signaling pathway and JAK-STAT signaling pathway. For Zn-CPS compared with CPS, response to zinc ion and cellular response to zinc ion biological process demonstrated zinc ion released from Zn-CPS participated in cell behaviors. Besides, Rap1 signaling pathway, which controls cell adhesion, migration and polarity, was activated in the DEGs of Zn-CPS with CPS as shown in Supplementary Fig. 8. Studies have revealed that the activation of Rap1 signaling pathway can inhibit polarization of M1 macrophage [45,46], indicating the addition of Zn could promote polarization of M2 macrophage through the activation of Rap1 signaling pathway in this work. Moreover, F7 (coagluation factor) also could activate complement and coagulation cascade pathway as shown in Supplementary Fig. 9, and the activation of complement and coagulation cascade pathway activate platelet activation to promote anti-inflammatory [47,48].

qRT-PCR, flow cytometry and ELISA analyses were then performed to analyze the immune response of RAW 264.7 to Fe-CPS and Zn-CPS at genetic and protein levels, and the results were shown in Figs. 3 and 4. Overall, both Fe-CPS and Zn-CPS have positive effects on reducing inflammatory reactions of RAW 264.7. Moreover, the inhibition effects of Fe and Zn on immune response showed a time difference trend,
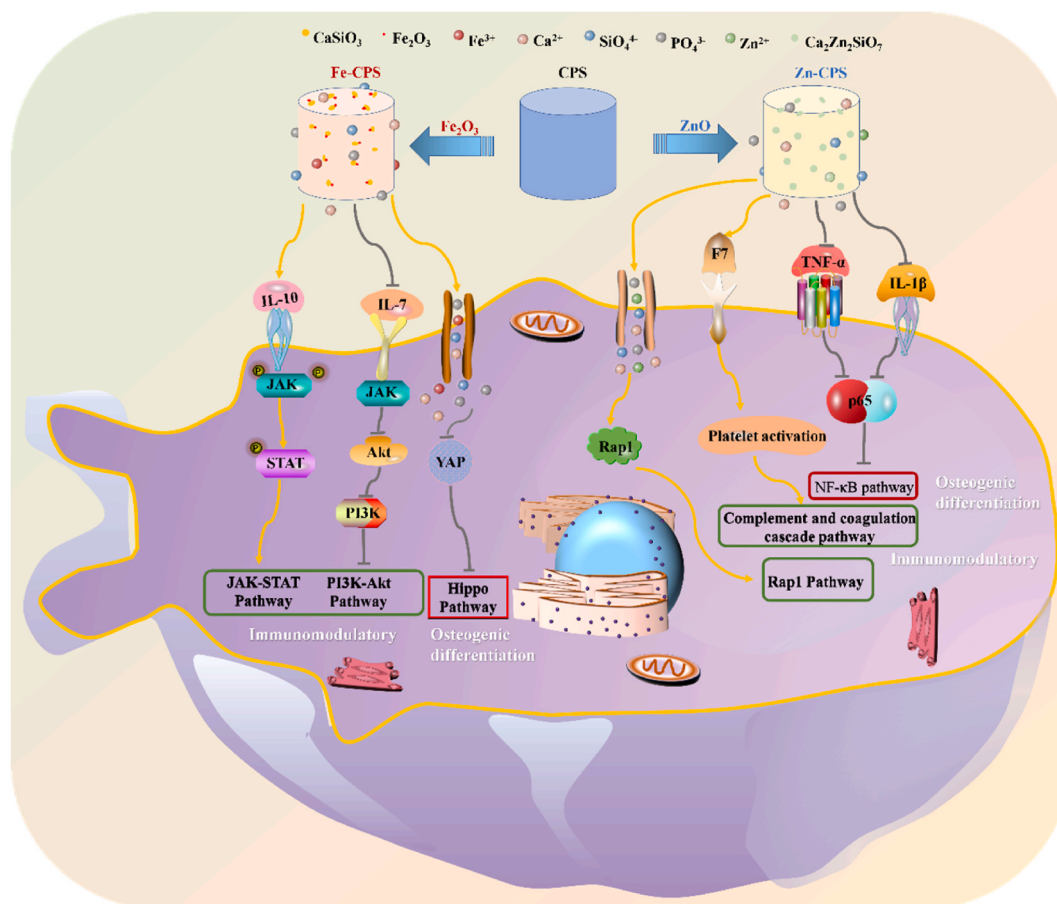
Fig. 8. Osteo-immunomodulation schematic diagram of Fe-CPS and Zn-CPS promoting osteogenesis.

indicating the immune microenvironment of Fe-CPS and Zn-CPS might also have time difference on osteogenesis. Conditioned mediums of different time points were prepared to verify the time difference characteristics of Fe-CPS and Zn-CPS bioceramics, and the results were shown in Figs. 5 and 6. The immune microenvironment of CPS, Fe-CPS and Zn-CPS presented a favorable effect and time difference trend on osteogenesis, specifically, both Zn-CPS-CM-2 and Zn-CPS-CM-4 could promote osteogenesis and osteogenic differentiation in shorter time, while in Fe-CPS group, only Fe-CPS-CM-4 had significantly positive effect on osteogenesis and osteogenic differentiation. In addition, CPS, Fe-CPS and Zn-CPS showed selectively promotion on expression of osteogenesis related genes, CPS could obviously promote the expression of SP7, CPS-CM-4 selectively promoted the expression of OPN, Fe-CPS-CM-4 significantly promoted the expression of COL1, while Zn-CPS clearly promoted the expression of ALP, and Zn-CPS-CM-4 selectively promoted the expression of VEGF, OCN and OPN. SP7, a transcription factor relates to bone development, which is indispensable to preosteoblastic cell differentiation [49]. Varanasi et al. have compared the osteogenic differentiation of 45S5 and 6P53-b, and found an enhanced expression of SP7 induced by Si element [50], which is consistent with our results.

Implantation experiments *in vivo* comprehensively evaluated the inflammatory response and osteogenic activity of Fe-CPS and Zn-CPS, as shown in Fig. 7, *in vivo* results were consistent with *in vitro* results, both Fe-CPS and Zn-CPS exhibited effective inhibition on inflammatory response and significant promotion on new bone formation. When it comes to the mechanism of Fe on osteogenesis, most studied have focused on ferroptosis, lactoferrin and magnetic iron oxide nanoparticles [51–53], as for Fe-doped biomaterials, the current studies only investigated the effects of Fe addition on mechanical and biological performances [54,55]. In humans, about 65 % of the total iron is

allocated in red blood cells (RBCs), 14 % in macrophages, and 5 % in bone marrow [56]. In M1 macrophages, studies have found iron can significantly reduce the secretion of IL-6, IL-1β, TNF-α, and iNOS produced by IFN-γ-polarized M1 macrophages, indicating moderate Fe can decrease immune inflammatory response [57]. Our research in this work also found the favorable effect of Fe on inhibiting immune inflammatory response *in vitro* and *in vivo*, moreover, Fe-CPS and its immune microenvironment might play a role on bone formation through Hippo signaling pathway. Yap is a downstream factor and negative regulator of Hippo signaling pathway, which plays a key role in proliferation and differentiation of osteoblasts [58,59]. Zhu et al. have proven that the upregulation of yap can activate Hippo signaling pathway to inhibit osteoblast growth [60]. Our works also verified the inhibition effect of yap on osteogenesis as shown in Fig. 6(e), the expression amount of yap and p-yap on Fe-CPS and Fe-CPS-CM groups were significantly lower than those of CPS and CPS-CM groups, indicating Fe element might promote osteogenesis via activating Hippo signaling pathway to suppress the expression of yap.

For Zn, evidences have proven that the incorporation of Zn significantly promotes the cell proliferation and osteogenic differentiation [61, 62]. It has also been reported that the addition of Zn can reduce the expression of TNF-α and IL-1β of M1, and promote the expression of TGF-β of M2, and thus create a favorable immune environment to accelerate bone formation [63–65]. In our present work, we also found the gene expression of TNF-α and INOS of M1 in Zn-CPS group significantly lower than those in CPS group, and the expression of CD206 and Arg1 of M2 in Zn-CPS group clearly higher than those in CPS group, which demonstrated Zn-CPS downregulated pro-inflammatory phenotype and upregulated anti-inflammatory phenotype of RAW264.7. In addition, both *in vitro* and *in vivo* results proved that the immune

microenvironment of Zn-CPS further promoted bone formation ability of CPS, and Western blot experiment discovered the amount of p65 and p-p65 were significantly lower than those of control group, indicating Zn-CPS and its immune microenvironment might improve osteogenesis through the activation of nuclear NF-κB signaling pathway. NF-κB signaling pathway is a transcription factor which is participate in regulating inflammation and immune response, while TNF-α and other inflammatory cytokines can activate NF-κB classical pathway. Moreover, studies have detected the activation of NF-κB signaling pathway is essential for osteoclast differentiation, and the inhibition of NF-κB signaling pathway simultaneously suppresses osteoclast and promote osteogenesis [66,67]. Masayoshi et al. have investigated the mechanism of Zn regulating bone formation and resorption, and results have shown that Zn achieves stimulating bone formation by suppressing the expression of TNF-α to inhibit NF-κB signaling pathway [68], which is consistent with our results.

Above all, both Fe-CPS and Zn-CPS bioceramics have extraordinary ability to promote bone formation, but, the mechanism of osteo-immunomodulation of Fe-CPS and Zn-CPS showed distinct. The diagram of Fe-CPS and Zn-CPS on osteo-immunomodulation was presented in Fig. 8, both Fe-CPS and Zn-CPS have good ability on osteo-immunomodulation, and Zn-CPS achieves promotion on polarization of M2 macrophage and osteogenesis *in vitro* and *in vivo* in a shorter time than Fe-CPS. Furthermore, the mechanism of Fe-CPS on osteo-immunomodulation are PI3K-Akt signaling pathway, JAK-STAT signaling pathway and Hippo signaling pathway. In comparison, Zn-CPS via the activation of Rap1 signaling pathway and complement and coagulation cascade pathway to promote the polarization of M2 macrophage, and then Zn-CPS with its immune microenvironment activate NF-κB signaling pathway to promote osteogenesis.

5. Conclusions

In conclusion, the immunomodulatory performance and its effect on osteogenesis of iron and zinc were investigated through preparing 1 wt% Fe_2O_3 added-CPS and 1 wt% ZnO added-CPS. Both *in vitro* and *in vivo* results confirmed that Fe-CPS and Zn-CPS could inhibit polarization of M1 macrophage and further improve osteogenesis, and presented a time difference trend of osteo-immunomodulation. Results indicate that the mechanism of Fe-CPS and Zn-CPS on osteo-immunomodulation are distinct, Fe-CPS achieves osteo-immunomodulation via PI3K-Akt signaling pathway, JAK-STAT signaling pathway and Hippo signaling pathway, while Rap1 signaling pathway, complement and coagulation cascade pathway and NF-κB signaling pathway are activated in Zn-CPS.

CRediT authorship contribution statement

Fanyan Deng: Writing – review & editing, Writing – original draft, Methodology, Investigation, Funding acquisition, Formal analysis, Data curation. **Xianzhuo Han:** Writing – original draft, Methodology, Investigation, Formal analysis, Data curation. **Yingqi Ji:** Investigation. **Ying Jin:** Investigation. **Yiran Shao:** Validation. **Jingju Zhang:** Writing – review & editing, Visualization, Supervision, Resources, Project administration. **Congqin Ning:** Writing – review & editing, Supervision, Resources, Project administration, Funding acquisition, Conceptualization.

Declaration of competing interest

We declare that we do not have no known competing financial interests or personal relationships that could have appeared to influence the work reported in this paper.

Data availability

Data will be made available on request.

Appendix A. Supplementary data

Supplementary data to this article can be found online at https://doi.org/10.1016/j.mtbio.2024.101086.

References

[1] J.O. Abaricia, N. Farzad, T.J. Heath, J. Simmons, L. Morandini, R. Olivares-Navarrete, Control of innate immune response by biomaterial surface topography, energy, and stiffness, Acta Biomater. 133 (2021) 58–73.

[2] J.E. Horton, L.G. Raisz, H.A. Simmons, J.J. Oppenheim, S.E. Mergenhagen, Bone resorbing activity in supernatant fluid from cultured human peripheral blood leukocytes, Science 177 (1972) 793–795.

[3] J.R. Arron, Y. Choi, Bone versus immune system, Nature 408 (2000) 535–536.

[4] H. Takayanagi, Osteoimmunology: shared mechanisms and crosstalk between the immune and bone systems, Nat. Rev. Immunol. 7 (2007) 292–304.

[5] F. Wei, Y.Q. Mu, R.P. Tan, S.G. Wise, M.M. Bilek, Y.H. Zhou, et al., Osteo-immunomodulatory role of interleukin-4-immobilized plasma immersion ion implantation membranes for bone regeneration, Acs Appl Mater Inter 15 (2023) 2590–2601.

[6] R.D. Devlin, S.V. Reddy, R. Savino, G. Ciliberto, G.D. Roodman, IL-6 mediates the effects of IL-1 or TNF, but not PTHrP or 1,25(OH)2D3, on osteoclast-like cell formation in normal human bone marrow cultures, J. Bone Miner. Res. 13 (1998) 393–399.

[7] M.H. Abdel Meguid, Y.H. Hamad, R.S. Swilam, M.S. Barakat, Relation of interleukin-6 in rheumatoid arthritis patients to systemic bone loss and structural bone damage, Rheumatol. Int. 33 (2013) 697–703.

[8] A. Wu, J. Shiloach, D. Alibek, L.Y. Li, C. Bradburne, K. Alibek, Anthrax lethal toxin inhibits the production of proinflammatory cytokines, J. Toxins 2013 (2013) 476909.

[9] S.M. Abdelmagid, M.F. Barbe, F.F. Safadi, Role of inflammation in the aging bones, Life Sci. 123 (2015) 25–34.

[10] J. Lee, H. Byun, S.K. Madhurakkat Perikamana, S. Lee, H. Shin, Current advances in immunomodulatory biomaterials for bone regeneration, Adv. Healthcare Mater. 8 (2019) e1801106.

[11] W. Liu, J. Li, M. Cheng, Q. Wang, K.W.K. Yeung, P.K. Chu, et al., Zinc-modified sulfonated polyetheretherketone surface with immunomodulatory function for guiding cell fate and bone regeneration, Adv. Sci. 5 (2018) 1800749.

[12] M.Z. Li, X.D. Guo, W.T. Qi, Z.Z. Wu, J.D. De Bruijn, Y. Xiao, et al., Macrophage polarization plays roles in bone formation instructed by calcium phosphate ceramics, J. Mater. Chem. B 8 (2020) 1863–1877.

[13] K.M. Hotchkiss, G.B. Reddy, S.L. Hyzy, Z. Schwartz, B.D. Boyan, R. Olivares-Navarrete, Titanium surface characteristics, including topography and wettability, alter macrophage activation, Acta Biomater. 31 (2016) 425–434.

[14] A. Vishwakarma, N.S. Bhise, M.B. Evangelista, J. Rouwkema, M.R. Dokmeci, A. M. Ghaemmaghami, et al., Engineering immunomodulatory biomaterials to tune the inflammatory response, Trends Biotechnol. 34 (2016) 470–482.

[15] C.B. He, Y.P. Hu, L.C. Yin, C. Tang, C.H. Yin, Effects of particle size and surface charge on cellular uptake and biodistribution of polymeric nanoparticles, Biomaterials 31 (2010) 3657–3666.

[16] J. Jeong, J.H. Kim, J.H. Shim, N.S. Hwang, C.Y. Heo, Bioactive calcium phosphate materials and applications in bone regeneration, Biomater. Res. 23 (2019).

[17] S.X. Xu, Q. Wu, J. Wu, H.M. Kou, Y.J. Zhu, C.Q. Ning, et al., Ultrasound-assisted synthesis of nanocrystallized silicocarnotite biomaterial with improved sinterability and osteogenic activity, J. Mater. Chem. B 8 (2020) 3092–3103.

[18] W. Duan, C.Q. Ning, T.T. Tang, Cytocompatibility and osteogenic activity of a novel calcium phosphate silicate bioceramic: silicocarnotite, J. Biomed. Mater. Res. 101 (2013) 1955–1961.

[19] F.Y. Deng, F. Wang, Z.W. Liu, H.M. Kou, G.F. Cheng, C.Q. Ning, Enhanced mechanical property of Ca-5(PO4)(2)SiO4 bioceramic by a biocompatible sintering aid of zinc oxide, Ceram. Int. 44 (2018) 18352–18362.

[20] F.Y. Deng, J.C. Rao, C.Q. Ning, Ferric oxide: a favorable additive to balance mechanical strength and biological activity of silicocarnotite bioceramic, J Mech Behav Biomed 109 (2020).

[21] F. Deng, Z. Bu, H. Hu, X. Huang, Z. Liu, C. Ning, Bioadaptable bone regeneration of Zn-containing silicocarnotite bioceramics with moderate biodegradation and antibacterial activity, Appl. Mater. Today 27 (2022) 101433.

[22] J. Zhang, F. Deng, X. Liu, Y. Ge, Y. Zeng, Z. Zhai, et al., Favorable osteogenic activity of iron doped in silicocarnotite bioceramic: in vitro and in vivo Studies, Journal of Orthopaedic Translation 32 (2022) 103–111.

[23] J.L. Roberts, A.D. Stein, The impact of nutritional interventions beyond the first 2 Years of life on linear growth: a systematic review and meta-analysis, Adv. Nutr. 8 (2017) 323–336.

[24] G. Gao, J. Li, Y. Zhang, Y.Z. Chang, Cellular iron metabolism and regulation, Adv. Exp. Med. Biol. 1173 (2019) 21–32.

[25] N.Z. Gammoh, L. Rink, Zinc in infection and inflammation, Nutrients 9 (2017).

[26] F. Velard, J. Braux, J. Amedee, P. Laquerriere, Inflammatory cell response to calcium phosphate biomaterial particles: an overview, Acta Biomater. 9 (2013) 4956–4963.

[27] B. Chen, Y.P. You, A.B. Ma, Y.J. Song, J. Jiao, L.T. Song, et al., Zn-incorporated TiO2 nanotube surface improves osteogenesis ability through influencing immunomodulatory function of macrophages, Int. J. Nanomed. 15 (2020) 2095–2118.

[28] A. DeRosa, A. Leftin, The iron curtain: macrophages at the interface of systemic and microenvironmental iron metabolism and immune response in cancer, Front. Immunol. 12 (2021) 614294.

[29] N.C. Winn, K.M. Volk, A.H. Hasty, Regulation of tissue iron homeostasis: the macrophage "ferrostat", Jci Insight 5 (2020).

[30] F.Y. Deng, F. Wang, Z.W. Liu, H.M. Kou, G.F. Cheng, C.Q. Ning, Enhanced mechanical property of Ca5(PO4)(2)SiO4 bioceramic by a biocompatible sintering aid of zinc oxide, Ceram. Int. 44 (2018) 18352–18362.

[31] Z.W.B. Zhang, W.B. Li, Y. Liu, Z.G. Yang, L.L. Ma, H. Zhuang, et al., Design of a biofluid-absorbing bioactive sandwich-structured Zn-Si bioceramic composite wound dressing for hair follicle regeneration and skin burn wound healing, Bioact. Mater. 6 (2021) 1910–1920.

[32] Y.H. Li, Y. Han, X.Y. Wang, J.L. Peng, Y.H. Xu, J. Chang, Multifunctional hydrogels prepared by dual ion cross-linking for chronic wound healing, Acs Appl Mater Inter 9 (2017) 16054–16062.

[33] E. El-Meliegy, M. Mabrouk, S.A.M. El-Sayed, B.M. Abd El-Hady, M.R. Shehata, W. M. Hosny, Novel Fe2O3-doped glass/chitosan scaffolds for bone tissue replacement, Ceram. Int. 44 (2018) 9140–9151.

[34] Y.R. Fu, K.S. Gao, R. Ji, Z.J. Yi, Differential transcriptional response in macrophages infected with cell wall deficient versus normal Mycobacterium tuberculosis, Int. J. Biol. Sci. 11 (2015) 22–30.

[35] L.Y. Gao, L. Zhu, C. Shen, X.M. Hou, Y.Y. Chen, L.L. Zou, et al., The transdermal cream of Formestane anti-breast cancer by controlling PI3K-Akt pathway and the tumor immune microenvironment, Front. Immunol. 14 (2023).

[36] A.H. Sprague, R.A. Khalil, Inflammatory cytokines in vascular dysfunction and vascular disease, Biochem. Pharmacol. 78 (2009) 539–552.

[37] D.A. Fruman, H. Chiu, B.D. Hopkins, S. Bagrodia, L.C. Cantley, R.T. Abraham, The PI3K pathway in human disease, Cell 170 (2017) 605–635.

[38] P.J. Murray, The JAK-STAT signaling pathway: input and output intergration, J. Immunol. 178 (2007) 2623–2629.

[39] L. Bao, X. Li, MicroRNA-32 targeting PTEN enhances M2 macrophage polarization in the glioma microenvironment and further promotes the progression of glioma, Mol. Cell. Biochem. 460 (2019) 67–79.

[40] L. Liu, X.X. Zhu, T.Y. Zhao, Y.Y. Yu, Y. Xue, H.J. Zou, Sirt1 ameliorates monosodium urate crystal-induced inflammation by altering macrophage polarization via the PI3K/Akt/STAT6 pathway, Rheumatology 58 (2019) 1674–1683.

[41] E. Vergadi, E. Ieronymaki, K. Lyroni, K. Vaporidi, C. Tsatsanis, Akt signaling pathway in macrophage activation and M1/M2 polarization, J. Immunol. 198 (2017) 1006–1014.

[42] T.D. Troutman, J.F. Bazan, C. Pasare, Toll-like receptors, signaling adapters and regulation of the pro-inflammatory response by PI3K, Cell Cycle 11 (2012) 3559–3567.

[43] J.M. Li, H. Zhang, Y.J. Zuo, MicroRNA-218 alleviates sepsis inflammation by negatively regulating VOPP1 via JAK/STAT pathway, Eur Rev Med Pharmaco 22 (2018) 5620–5626.

[44] F. Cordes, E. Lenker, T. Weinhage, L.J. Spille, D. Bettenworth, G. Varga, et al., Impaired IFN-gamma-dependent STAT3 activation is associated with dysregulation of regulatory and inflammatory signaling in monocytes of ulcerative colitis patients, Inflamm. Bowel Dis. 27 (2021) 887–901.

[45] Y. Liang, X.L. Sun, M.J. Wang, Q.M. Lu, M.R. Gu, L. Zhou, et al., PP2Ac alpha promotes macrophage accumulation and activation to exacerbate tubular cell death and kidney fibrosis through activating Rap1 and TNF alpha production, Cell Death Differ. 28 (2021) 2728–2744.

[46] R. Dou, X.L. Zhang, X.D. Xu, P. Wang, B.Z. Yan, Mesenchymal stem cell exosomal tsRNA-21109 alleviate systemic lupus erythematosus by inhibiting macrophage M1 polarization, Mol. Immunol. 139 (2021) 106–114.

[47] S.P. Jackson, R. Darbousset, S.M. Schoenwaelder, Thromboinflammation: challenges of therapeutically targeting coagulation and other host defense mechanisms, Blood 133 (2019) 906–918.

[48] J.N. Kizhakkedathu, E.M. Conway, Biomaterial and cellular implants: foreign surfaces where immunity and coagulation meet, Blood 139 (2022) 1987–1998.

[49] K. Nakashima, X. Zhou, G. Kunkel, Z. Zhang, J.M. Deng, R.R. Behringer, et al., The novel zinc finger-containing transcription factor osterix is required for osteoblast differentiation and bone formation, Cell 108 (2002) 17–29.

[50] V.G. Varanasi, T. Odatsu, T. Bishop, J. Chang, J. Owyoung, P.M. Loomer, Enhanced osteoprogenitor elongated collagen fiber matrix formation by bioactive glass ionic silicon dependent on Sp7 (osterix) transcription, J. Biomed. Mater. Res. 104 (2016) 2604–2615.

[51] J.C. Yang, J.W. Wu, Z.F. Guo, G.J. Zhang, H. Zhang, Iron oxide nanoparticles combined with static magnetic fields in bone remodeling, Cells-Basel 11 (2022).

[52] Y.Z. Ye, A. Chen, L. Li, Q.C. Liang, S.Y. Wang, Q.Q. Dong, et al., Repression of the antiporter SLC7A11/glutathione/glutathione peroxidase 4 axis drives ferroptosis of vascular smooth muscle cells to facilitate vascular calcification, Kidney Int. 102 (2022) 1259–1275.

[53] M. Liu, F.J. Fan, P.J. Shi, M.L. Tu, C.P. Yu, C.X. Yu, et al., Lactoferrin promotes MC3T3-E1 osteoblast cells proliferation via MAPK signaling pathways, Int. J. Biol. Macromol. 107 (2018) 137–143.

[54] X. Pan, J. Huang, K.L. Zhang, Z.J. Pei, Z.F. Ding, Y.X. Liang, et al., Iron-doped brushite bone cement scaffold with enhanced osteoconductivity and antimicrobial properties for jaw regeneration, Ceram. Int. 47 (2021) 25810–25820.

[55] A.P. Wang, W.Q. Du, Y.A. Zhang, Z.L. Zhang, Y.H. Zou, J.P. Luan, et al., Iron-doped calcium silicate bone cement loaded with carboxymethyl chitosan for bone tissue engineering repair materials, J. Sol. Gel Sci. Technol. 106 (2023) 44–53.

[56] C. Scott, G. Arora, K. Dickson, C. Lehmann, Iron chelation in local infection, Molecules 26 (2021). Basel, Switzerland.

[57] Z.S. Gan, Q.Q. Wang, J.H. Li, X.L. Wang, Y.Z. Wang, H.H. Du, Iron reduces M1 macrophage polarization in RAW264.7 macrophages associated with inhibition of STAT1, Mediat. Inflamm. 2017 (2017) 8570818.

[58] Y. Tang, T. Feinberg, E.T. Keller, X.Y. Li, S.J. Weiss, Snail/Slug binding interactions with YAP/TAZ control skeletal stem cell self-renewal and differentiation, Nat. Cell Biol. 18 (2016) 917–929.

[59] J.X. Pan, L. Xiong, K. Zhao, P. Zeng, B. Wang, F.L. Tang, et al., YAP promotes osteogenesis and suppresses adipogenic differentiation by regulating beta-catenin signaling, Bone Res. 6 (2018).

[60] W.Q. Zhou, P.P. Ming, J. Qiu, S.Y. Shao, Y.J. Yu, J.X. Chen, et al., Effect of titanium ions on the Hippo/YAP signaling pathway in regulating biological behaviors of MC3T3-E1 osteoblasts, J. Appl. Toxicol. 38 (2018) 824–833.

[61] D.X. Ke, S. Tarafder, S. Vahabzadeh, S. Bose, Effects of MgO, ZnO, SrO, and SiO2 in tricalcium phosphate scaffolds on in vitro gene expression and in vivo osteogenesis, Mater. Sci. Eng., C 96 (2019) 10–19.

[62] A.S. Tiffany, D.L. Gray, T.J. Woods, K. Subedi, B.A.C. Harley, The inclusion of zinc into mineralized collagen scaffolds for craniofacial bone repair applications, Acta Biomater. 93 (2019) 86–96.

[63] F. Velard, J. Braux, J. Amedee, P. Laquerriere, Inflammatory cell response to calcium phosphate biomaterial particles: an overview, Acta Biomater. 9 (2013) 4956–4963.

[64] B. Chen, Y. You, A. Ma, Y. Song, J. Jiao, L. Song, et al., Zn-incorporated TiO(2) nanotube surface improves osteogenesis ability through influencing immunomodulatory function of macrophages, Int J Nanomedicine 15 (2020) 2095–2118.

[65] R.R. Zhang, X.J. Liu, Z.Y. Xiong, Q.L. Huang, X. Yang, H. Yan, et al., The immunomodulatory effects of Zn-incorporated micro/nanostructured coating in inducing osteogenesis, Artif Cell Nanomed B 46 (2018) S1123–S1130.

[66] E. Jimi, N. Takakura, F. Hiura, I. Nakamura, S. Hirata-Tsuchiya, The role of NF-kappaB in physiological bone development and inflammatory bone diseases: is NF-kappaB inhibition "killing two birds with one stone", Cells-Basel 8 (2019).

[67] M. Jarosz, M. Olbert, G. Wyszogrodzka, K. Młyniec, T. Librowski, Antioxidant and anti-inflammatory effects of zinc. Zinc-dependent NF-κB signaling, Inflammopharmacology 25 (2017) 11–24.

[68] M. Yamaguchi, M.N. Weitzmann, Zinc stimulates osteoblastogenesis and suppresses osteoclastogenesis by antagonizing NF-kappaB activation, Mol. Cell. Biochem. 355 (2011) 179–186.